Icarus 430 (2025) 116484

Contents lists available at ScienceDirect

Icarus

journal homepage: www.elsevier.com/locate/icarus

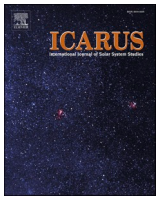

Low thermal inertia of (162173) Ryugu a result of horizontal cracks in boulders

Maximilian Hamm [a,b,*], Moritz Strauß [a], Matthias Grott [b], Jörg Knollenberg [b], Robert Luther [c], Jens Biele [d], Hiroki Senshu [e]

[a] Planetary Sciences and Remote Sensing, Institute of Geological Sciences, Freie Universität Berlin, Malteserstr. 74-100, 12249 Berlin, Germany
[b] Institute of Planetary Research, German Aerospace Center (DLR), Rutherfordstr. 2, 12489 Berlin, Germany
[c] Museum für Naturkunde – Leibniz Institute for Evolution and Biodiversity Science, Invalidenstraße 43, 10115 Berlin, Germany
[d] Microgravity User Support Center, German Aerospace Center (DLR RB-MUSC), Linder Höhe 29, 51147 Cologne, Germany
[e] Chiba Institute of Technology, Planetary Exploration Research Center, 2-17-1 Tsudanuma, Narashino-city, Chiba, Japan

ARTICLE INFO

Keywords:
Asteroid surfaces
Near-earth objects
Regolith
Remote sensing
Planetary science

ABSTRACT

Observations of the diurnal variations of the surface temperature of asteroid (162173) Ryugu from orbit and on the surface were performed by the Haybusa2 spacecraft and MASCOT lander. A low thermal inertia of the boulders on Ryugu was derived from these temperature variations and interpreted as the consequence of high porosity. Samples of Ryugu returned to Earth by Hayabusa2 showed higher thermal inertia when investigated by microscopic thermography. Here, we apply a simple thermal model, considering a horizontal fracture interrupting the heat flow into the surface, and investigate whether the low thermal inertia of Ryugu's boulders might be caused by fractures rather than high porosity. We find that the diurnal temperature variations on Ryugu observed by MARA can be partially explained by introducing a single horizontal crack at 9 mm depth below the surface observed by MARA.

1. Introduction

The JAXA Hayabusa2 sample return mission investigated asteroid (162173) Ryugu via remote sensing (Watanabe et al., 2019), deployed the DLR/CNES MASCOT lander (Ho et al., 2021), performed an artificial impact experiment (Arakawa et al., 2020) and returned samples to Earth (Yada et al., 2022). Ryugu is a rubble-pile asteroid with similarities to aqueously altered carbonaceous chondrites, in particular CI chondrites (Kitazato et al., 2021, Hamm et al., 2022, Nakamura et al., 2022, Yokoyama et al., 2023). One of the biggest surprises was the prevalence of boulders and decimeter-sized pebbles on the surface and the deficiency of smaller particles (Jaumann et al., 2019; Sugita et al., 2019). Such smaller particles were expected to dominate the surface based on thermal inertia estimates from telescopic infrared observations (Müller et al., 2017). The MASCOT radiometer MARA and the main spacecraft's TIR infrared imager confirmed the thermal inertia estimates from telescopic observations despite the boulder-dominated surface (Grott et al., 2019; Okada et al., 2020). The low thermal inertia was confirmed to be an intrinsic property of the boulders themselves (Grott et al., 2019; Sakatani et al., 2021; Hamm et al., 2022). More specifically, the presence of a layer of dust masking the thermophysical properties of the boulder was limited to small patches of thin dust layers, or no dust at all (Biele et al., 2019; Hamm et al., 2023). In contrast to these in-situ results, the analysis of sample fragments by lock-in thermography resulted in much larger thermal inertias more comparable to that of meteorite samples (Ishizaki et al., 2023).

In this study, we attempt to reconciliate the results from spacecraft observations and laboratory analysis by expanding our thermophysical model to incorporate horizontal fractures in the surface material. This procedure has been proposed by Elder, 2024. We investigate if it is possible to explain the MARA observations with a fractured boulder of higher bulk thermal inertia. This work also has implication on the regolith gardening on asteroids like Ryugu, as weak and porous boulders would respond differently to micro-meteorite impacts than fractured boulders with low porosity (Cambioni et al., 2021).

* Corresponding author at: Planetary Sciences and Remote Sensing, Institute of Geological Sciences, Freie Universität Berlin, Malteserstr. 74-100, 12249 Berlin, Germany.
E-mail addresses: Maximilian.Hamm@fu-berlin.de (M. Hamm), Matthias.Grott@dlr.de (M. Grott), Jorg.Knollenberg@dlr.de (J. Knollenberg), Robert.Luther@mfn.berlin (R. Luther), Jens.Biele@dlr.de (J. Biele), senshu@perc.it-chiba.ac.jp (H. Senshu).

https://doi.org/10.1016/j.icarus.2025.116484
Received 24 October 2024; Received in revised form 26 January 2025; Accepted 27 January 2025
Available online 30 January 2025

2. Methods

We start from the 1D-thermal model as used in Hamm et al., 2020. The heat conduction equation is solved for a 1D grid of 200 points from $x_0 = 0$ to $x_{200} = 0.166$ m. The grid points are distributed in increasing intervals: 0.05 mm for $x < 1$mm, 0.1 mm for $x < 2$mm, 0.5 mm for $x < 7$ mm, and 1 mm for $x \geq 7$mm. At the lower boundary condition, the flux into the computational domain is set to zero. The upper boundary condition is given by the surface energy balance

$$I\,(1-A) = \sigma\varepsilon_{eff}T^4(x=0,t) - k\frac{\partial T}{\partial x}_{x=0}$$

With temperature T, Stephan-Boltzmann constant σ, Bond albedo A, and thermal conductivity k. Illumination I is calculated by averaging over those facets of a boulder shape model within the MARA field of view, while weighting each facets contribution by the view factor of the facet to the MARA detector (Hamm et al., 2022). To reduce the computational costs, we incorporate thermal radiation of the surrounding by assuming the environment of the surrounding to be on average equal to the temperature of the simulated spot. Then, the energy input from the environment is $-f\varepsilon T^4$, where f parameterizes the view factor to the surrounding terrain. We then combine this expression with the radiation of the simulated spot to $\sigma\varepsilon_{eff}T^4(x=0,t)$ as described in Hamm et al., 2023. The surface roughness introduces temperature heterogeneity in the MARA field of view resulting in deviation of the observed flux from a Lambertian emitter that are depending on the observation and insolation geometry. During nighttime observations this effect becomes negligible (Giese and Kührt, 1990; Grott et al., 2019; Hamm et al., 2022). Hamm et al., 2022 showed that the boulder shape model accounts for most of the roughness effect and Hamm et al., 2023 showed that the further simplification by introducing f as described above accounts for most of the effect.

In this study, we introduce cracks into the model by considering only radiative heat transport across them. In this case, the heat conduction equation is given by

$$\rho c_p\frac{\partial T(x,t)}{\partial t} = \sigma\left(T^4(x_d,t) - T^4(x_u,t)\right)$$

for $x_u \leq x \leq x_d$, with x_d the grid point defining the lower edge of the fracture and x_u the upper edge, i.e., closer to the surface. Density is given by ρ, specific heat by c_p. Elsewhere on the grid, heat transport is governed by conduction and given by

$$\rho c_p\frac{\partial T(x,t)}{\partial t} = k\frac{\partial^2 T(x,t)}{\partial x^2}$$

This adaption accounts for radiative transfer across a horizontal fracture that blocks the conductive heat transfer. It is valid locally within the material if the fracture is spread far enough to neglect conduction over contact points. Also, the model assumes that the fracture is wide enough, i.e., larger than a few μm, to neglect heat transfer contributions by evanescent waves (Persson and Biele, 2022). Under these assumptions, the width of the crack does not influence the heat transfer across the cracks.

The heat conduction equation is solved by a commercial solver from *Numerical Algorithms Group* (*n*AG®), using a backward integration scheme. We vary the depth of the crack h_c by setting $x_u = h_c$ and vary the thermal conductivity k of the bulk material. For specific heat capacity and density, we use the bulk values of the Ryugu samples as reported in Nakamura et al., 2022: $c_p = 865$ J/K (at 298 K) and $\rho = 1800$ kg/m^3. The thermal conductivity is varied such that the thermal inertia $TI = \sqrt{k\rho c_p}$ varies from 300 to 1000 Jm^{-2}K^{-1}s$^{-1/2}$. This approach assumes that k, ρ, c_p are independent of temperature above and below the fracture. Analysis of carbonaceous chondrites found only little dependence of k and c_p on temperature above 200 K (Opeil et al., 2020). Assuming temperature independence of thermophysical parameters is a common simplification proven in previous works on Ryugu that showed that introduction of temperature dependency did not improve the fitting quality of the respective models (e.g. Grott et al., 2019; Hamm et al., 2020; Hamm et al., 2022; Shimaki et al., 2020; Senshu et al., 2022).

3. Results

The presence of a horizontal fracture in the modelled subsurface significantly alters the diurnal surface temperature variations. The reduced heat flow results in higher diurnal amplitudes. Also, the lag of the diurnal temperature variation and insolation, i.e., the time between maximum insolation during noon and maximum temperature, decreases if a fracture is present. Thus, the diurnal temperature curve becomes similar to those of a surface with lower thermal inertia. The increase in amplitude and decrease in lag depend on the position of the fracture. The closer the fracture is to the surface, the more the thermal inertia is reduced. Fig. 1 shows results of the thermophysical model in comparison to the surface temperature observations by MARA (Grott et al., 2023). For reference we show the result for a simplified thermal model with no fracture and a thermal inertia of 300 J m^{-2} K^{-1} s$^{-1/2}$ (Hamm et al., 2023). While amplitude and lag get very close, the overall shape of the cooling curves cannot entirely be reproduced within measurement uncertainties.

The dependence of temperature amplitude and lag on the position of the fracture is shown in Fig. 2. The trends are non-linear and converge towards amplitude and lag of the bulk materials if the crack is placed about two diurnal skin depths below the surface. This is expected as diurnal temperature variation should be dominated by the subsurface properties within the skin depth. Beyond the skin depth the sub-surface temperature variations become smaller and smaller until the temperature reaches an equilibrium. Unlike stationary instruments like MARA, infrared instruments on orbiters can usually only observe fractions of the diurnal temperature variation. If only temperature range or temperature lag with respect to insolation are used to determine thermal inertia, a model considering a crack or one with lower thermal inertia cannot be distinguished.

We vary depth of fracture and bulk thermal inertia, i.e. the thermal inertia of the material above and below the crack, varying k and keeping

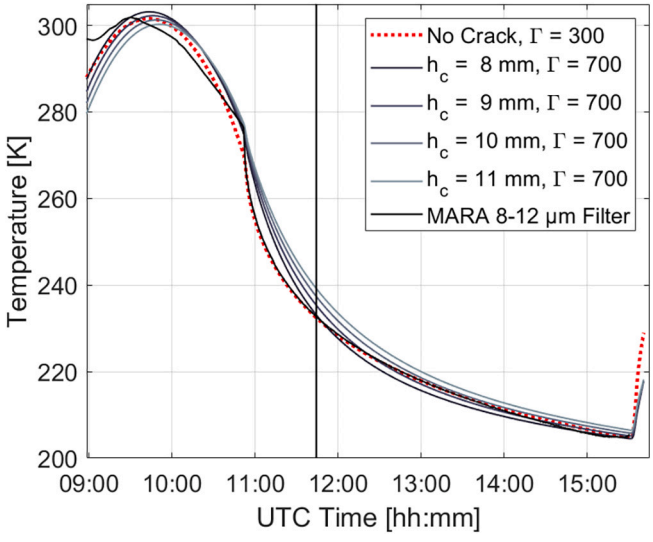

Fig. 1. Surface temperature derived from the MARA 8–12 μm filter in comparison to result of the thermophysical model with various parameters. The best fitting model is shown in red for a homogenous 1D-model with no fractures. In shades of gray, is the model assuming a fracture at depth h and a much higher bulk thermal inertia. The vertical line indicates the time from where data is included for fitting. (For interpretation of the references to colour in this figure legend, the reader is referred to the web version of this article.)

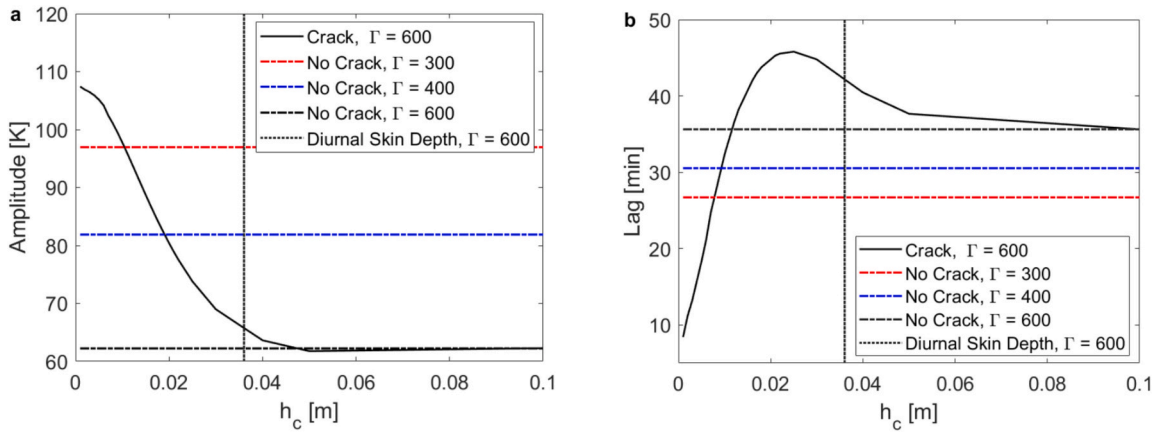

Fig. 2. Parameter of diurnal temperature variation as function of fracture depth a) Amplitude of the diurnal temperature variation calculated using the simplified thermal model assuming a horizontal fracture as a function of depth of the fracture with a bulk thermal inertia of 600 J $m^{-2}K^{-1}s^{-1/2}$. b) as a) but showing the lag between maximum temperature and maximum insolation. In both figures, dash-dotted horizontal lines show the amplitude and lag of temperature variations for a thermal model assuming the bulk thermal inertias of 300, 400, and 600 J $m^{-2}K^{-1}s^{-1/2}$ not including a crack, vertical dotted lines indicate the skin-depth for a thermal inertia of 600 J $m^{-2}K^{-1}s^{-1/2}$.

c_p and ρ constant. In order to derive the best-fitting crack depth we attempt to fit the nighttime observations of MARA, considering the last 453 data points. At these times, roughness effects become negligible. Fig. 3a shows the reduced χ^2 values across the parameter space. Values of $\chi^2/dof > 20$ are not plotted, where *dof* are the degrees of freedom, here 451. Usually, a good fit should have a have $\chi^2/dof \cong 1$. Such values are obtained for models with a fracture so deep that it does not alter the surface temperature and a bulk thermal inertia of roughly 300 J m^{-2} K^{-1} $s^{-1/2}$. This is equivalent to assuming no fracture at all and reproduces earlier modelling results (Hamm et al., 2020; Hamm et al., 2022; Grott et al., 2019). A second minimum appears for fracture depth at 9 mm for bulk thermal inertia between 600 and 800 J m^{-2} K^{-1} $s^{-1/2}$. Here, the χ^2/dof is between 2.5 and 3.5. Given the simplicity of the model and the discrepancy of earlier works to laboratory measurements of thermal diffusivity (Ishizaki et al., 2023), we accept these solutions nevertheless.

The boulders on the surface of Ryugu vary in thermal inertia. Shimaki et al. (2020) published a map of thermal inertia on Ryugu and Sakatani et al. (2021) published a histogram of thermal inertia of individual boulders. Both assume homogenous half-spaces in their thermal model, i.e., not including cracks. These works analyzed the TIR observations, observing only illuminated terrain. The effect of surface roughness was accounted for when estimating the thermal inertia. Thus, the reported thermal inertias are independent material properties and can be directly compared to our study. We investigate which fracture depth fits best a model without fracture. This is equivalent to investigating the apparent thermal inertia of a fractured boulder with higher thermal inertia of the intact material. The model results are converted into flux as would be observed by the MARA instrument. Fig. 3b shows the fracture depth for models with material's thermal inertia of 500 and 900 J m^{-2} K^{-1} $s^{-1/2}$ that fit the temperature variation calculated with the model not including a crack with thermal inertias from 200 to 400 J m^{-2} K^{-1} $s^{-1/2}$. This range covers the majority of the thermal inertia range of boulders as reported by Sakatani et al. (2021). As expected, the lower the thermal inertia of the homogenous model, the closer the crack has to be to the surface in a model with higher thermal inertia. The corresponding crack depths range from 1 to 17 mm. None of the fits are perfect and as for the MARA data, not the entire curve can be

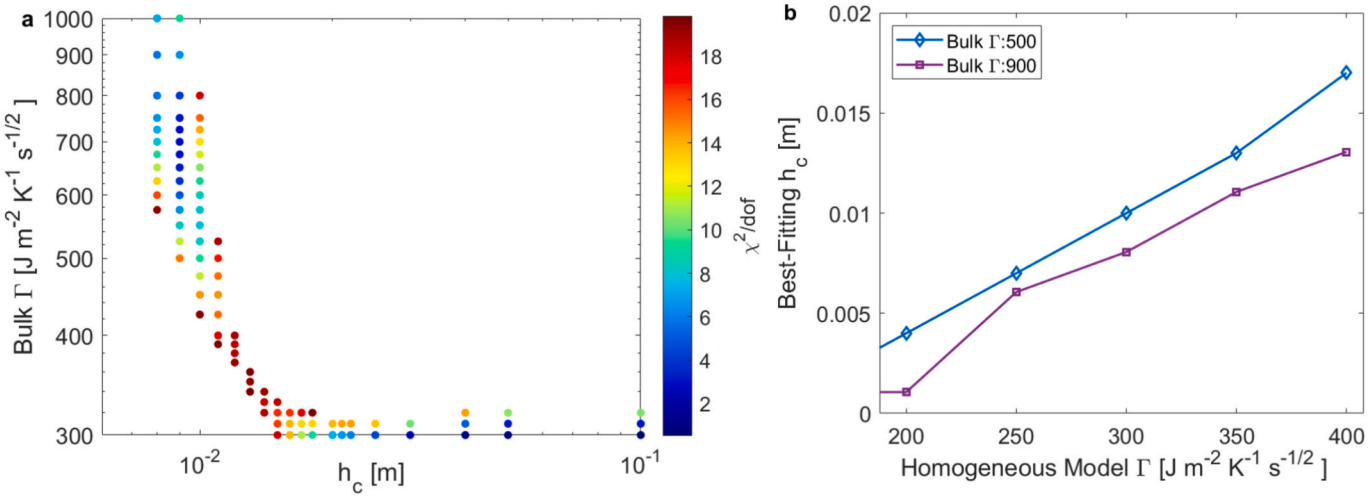

Fig. 3. Results of model fitting. a) reduced χ^2-value for range of h_c and Γ fitting the last 453 data points of the MARA 8–12 μm Filter observations. **b)** Fitting the diurnal temperature curve calculated with a model not assuming a crack with a model assuming a crack, varying the depth of that crack. Simulation results are converted to observed flux using the MARA calibration and the part of the curve used for fitting is identical to a). Y-axis shows the best-fitting depth of the crack for a bulk thermal inertia of 500 and 900 J $m^{-2}K^{-1}s^{-1/2}$ X-axis shows the thermal inertia used in the model without assuming a crack. The plot shows that, e.g., a model assuming 500 J $m^{-2}K^{-1}s^{-1/2}$ with a crack at 1 cm depth will have a similar temperature variation as a model assuming 300 J $m^{-2}K^{-1}s^{-1/2}$ and no crack.

reproduced. A thermal inertia below 200 J m^{-2} K^{-1} $s^{-1/2}$ cannot be explained within the limits of our fracture model.

4. Discussion

Introducing a fracture in the subsurface interrupts the heat flow since radiative heat transfer is significantly less efficient than solid conduction at relevant temperatures. Consequently, the solar energy absorbed by the surface has less space to dissipate and the surface above the cracks heats up faster. At night, the trapped heat close to the surface is inefficiently heated from below, resulting in faster cooling. It is therefore not the introduction of a T-dependent thermal conductivity but the interruption of heat flow within the diurnal skin depth that changes the diurnal temperature variation. Qualitatively, the results are similar to those of a 3D thermal model of particle monolayers on rock substrate as reported in Ryan et al., 2024. In that same study, the authors concluded that since no dust particles were observed during close-up observations of boulders on Bennu with low apparent thermal inertia, a high degree of fracturing could explain the low thermal inertia of the observed boulders.

Our model does not offer a perfect fit. The last 4 h of the night can be well reproduced using this model while the temperatures around sunset cannot. This could be due to the simplicity of the model, since, in a real boulder, the fractures are forming networks with some solid conduction at contact points. Only a fraction of the cracks within Ryugu's boulder will be parallel to the surface. Elder, 2023 showed that in preliminary results vertical cracks, i.e. parallel to the heat flow, will have only a small influence on the thermal conductivity, while pointing at the need for further studies to verify that hold for various widths and depths of vertical cracks. The results showed that the position of the first crack interrupting the heat flow, i.e. parallel to the illuminated surface, will be most relevant for the reduction of thermal conductivity (Elder, 2023; Elder, 2024). We also omit the effect of heat transfer by evanescent waves as described by Persson and Biele, 2022.

Applying Occam's Razor, the simplest model assuming a homogenous sub-surface with low thermal conductivity, which also fits the data best, would be the preferable explanation for the observations of MARA on Ryugu. However, since the analysis of Ishizaki et al., 2023, shows that the investigated millimeter-sized samples of Ryugu have a higher bulk thermal conductivity, we are left with few options: First, the samples could be more compact fragments of boulders, with the more porous material observed by MARA and TIR being lost during sampling. Second, the surface of the boulder might be streaked by fractures where those parallel to the surface obstruct the heat flow and lower the apparent thermal inertia. Third, rather than fractures, mono- or bilayers of dust particles cover the boulder and the interruption of heat flow at the particle-substrate interface reduces the apparent thermal inertia as reported by Ryan et al., 2024 for asteroid Bennu. The effect of such monolayers has not been modelled for Ryugu yet. Layers of dust could explain some difference between Ryugu sample C0137 MIR spectra and MARA observations. However, for such an effect the layer of dust needs to be more than a few layers of particles thick and such a thick layer covering any substantial fraction of the MARA field of view could be excluded (Hamm et al., 2023). Furthermore, no such layer was observed by MASCOT camera images (Jaumann et al., 2019). Consequently, dust is unlikely to produce the low observed thermal inertia. Contrarily, the obstruction of heat flow by fractures was observed in Ryugu samples (Ishizaki et al., 2023).

Fractures in the shallow sub-surface of boulders could be the result of a continuous influx of impactors of small size. Depending on the size ratio of the impactor to the boulders that were hit, these events form small craters with radial and concentric fractures below the crater floor, or they disrupt the entire boulder. In the latter case, it can be expected to find fractures in the impact generated boulder fragments. In the last years, a series of laboratory experiments into competent rock have been conducted where the target materials vary in terms of porosity and strength, including materials like sandstone, quartzite, marble, granite, tuff and also asteroid (Carbonaceous Chondrite) simulant (Kenkmann et al., 2018; Avdellidou et al., 2020; Kurosawa et al., 2022; Hamann et al., 2023). The weaker materials, the asteroid simulant and the tuff, are also the ones with the largest bulk porosity of ~26 % and 43 %, respectively, while sandstone shows a porosity of 23.1 %, and marble and quartzite are non-porous. The resulting craters are strength dominated and show significant spallation zones. An inner deeper crater is surrounded by a relatively wide and shallow zone (e.g. Poelchau et al., 2013). The formation of fractures and spall depends on the target properties. For non-porous materials, fractures have been observed in radial and concentric direction from the crater floor, and spall fractures close to the impact facing surface (Winkler et al., 2018; Hamann et al., 2023; Polanskey and Ahrens, 1990; Hörz, 1969). With increasing porosity, a decrease of crater volumes and cratering efficiency is observed with respect to non-porous targets (Poelchau et al., 2013). For sandstone targets, fractures have been mostly observed as spallation fractures, but, in contrast to the non-porous targets, were not so developed underneath the crater floor (Buhl et al., 2012). Nevertheless, material damage was observed for sandstone targets far below the crater floor (Raith et al., 2018). Even though boulders on Ryugu are expected to be weaker than rocks on Earth, strength dominated cratering with spallation fractures parallel to the surface and subsurface modification is a feasible process for the formation of fractures that alter the thermal inertia of a single boulder.

Besides impacts, the diurnal temperature cycles cause stress fields that can introduce fractures in the surface material. The process is known as thermal fatigue and has been postulated as an important factor of weathering surface material on airless bodies (Delbo et al., 2014; Guy et al., 2024). Rozitis et al., 2020 refer to micro-strutural cracks as one possible reason for the low thermal inertia on Bennu and in particular at its equator. Thermal fatigue is also the likely cause of fractures in rocks on Dimorphos observed by the DART mission (Lucchetti et al., 2024). As shown by Molaro et al., 2017, thermal stresses can cause the cracks parallel to the surface that we cover in this study and that would reduce the overall thermal conductivity of the boulders on asteroids). These parallel cracks can lead to exfoliation of smaller fragments, which is one mechanism that could explain the ejection of particles on Bennu (Molaro et al., 2020). On Ryugu, such an ejection was not observed, but thermal fracturing could occur on Ryugu with the fragments remaining on the surface. In particular, recent work by Schirner et al. (2024) showed that the north-south orientation of large cracks on Ryugu's boulders are strong signs for thermal fatigue. Daoud et al., 2020 found that thermal fatigue has a memory effect where damage during past exposure to temperature cycles accumulates over time. Given that Ryugu might have experienced substantial heating on past orbits, the boulders on Ryugu might have experienced high degrees of thermal fatigue over the course of time (Michel and Delbo, 2010).

5. Conclusion

The reconciliation of observations of Hayabusa2 and MASCOT on the one hand, and laboratory analysis of the samples from Ryugu on the other hand, remains a challenge. Further analysis of the thermophysical properties of the samples and advances in thermal modelling are necessary. We show that fractures obstructing the heat flow as observed in returned samples can reduce the apparent thermal inertia and partially explain the MARA observations. Such fractures can form in the vicinity of impact craters and due to thermal fatigue. Analysis of the fracture networks within various samples of Ryugu, Bennu, but also meteorites and correlation with heat-flow experiments such as the lock-in thermography by Ishizaki et al., 2023 are important next steps. Such measurements could then substantially improve modelling efforts and thus advance the interpretation of mid-infrared observations, e.g. from TIRI onboard the ESA Hera mission to (65803) Didymos.

CRediT authorship contribution statement

Maximilian Hamm: Writing – original draft, Validation, Software, Methodology, Funding acquisition, Conceptualization. **Moritz Strauß:** Software, Formal analysis. **Matthias Grott:** Writing – original draft, Validation. **Jörg Knollenberg:** Writing – original draft, Validation. **Robert Luther:** Writing – original draft. **Jens Biele:** Writing – original draft, Validation. **Hiroki Senshu:** Writing – review & editing, Methodology.

Declaration of competing interest

The authors declare that they have no known competing financial interests or personal relationships that could have appeared to influence the work reported in this paper.

Acknowledgments

M.H. is funded by the Deutsche Forschungsgemeinschaft (DFG, German Research Foundation) – Project-No. 497966340.

Data availability

The MARA data used in this study is available on NASA PDS (using URL: doi: 10.17597/isas.darts/hyb2-01000).

References

Arakawa, M., et al., 2020. An artificial impact on the asteroid (162173) Ryugu formed a crater in the gravity-dominated regime. Science 368, 67–71.
Avdellidou, C., et al., 2020. Very weak carbonaceous asteroid simulants I: mechanical properties and response to hypervelocity impacts. Icarus 341, 113648.
Biele, J., et al., 2019. Effect of dust layers on thermal emission from airless bodies. Prog. Earth Plan. Sci. 6, 48.
Buhl, E., et al., 2012. Deformation of dry and wet sandstone targets during hypervelocity impact experiments, as revealed from the MEMIN program. Meteorit. Planet. Sci. 48, 71–86.
Cambioni, S., et al., 2021. Fine-regolith production on asteroids controlled by rock porosity. Nature 598, 49–52. https://doi.org/10.1038/s41586-021-03816-5.
Daoud, A., et al., 2020. Microstructural controls on thermal crack damage and the presence of a temperature-memory effect during cyclic thermal stressing of rocks. GRL 47, 88693.
Delbo, M., et al., 2014. Thermal fatigue as the origin of regolith on small asteroids. Nature 508 (7495), 233–236.
Elder, C.M., 2023. Boulders on Bennu: investigating the structure of low thermal inertia rock using thermal modeling. In: *54th LPSC*, The Woodlands, TX. https://www.hou.usra.edu/meetings/lpsc2023/pdf/2639.pdf.
Elder, C.M., 2024. Thermal inertia on Bennu: explanation of remote sensing observations and predictions for samples. In: *55th LPSC*, The Woodlands, TX. https://www.hou.usra.edu/meetings/lpsc2024/pdf/2590.pdf.
Giese, B., Kührt, E., 1990. Theoretical interpretation of infrared measurements at Deimos in the framework of crater radiation. Icarus 88, 372–379.
Grott, M., et al., 2019. Low thermal conductivity boulder with high porosity identified on C-type asteroid (162173) Ryugu. Nat. Astron. **3**, 971–976.
Grott, M., et al., 2023. Hayabusa2 MASCOT MARA Radiometer Bundle V1.0. NASA Planetary Data System. https://doi.org/10.17597/isas.darts/hyb2-01000.
Guy, L., et al., 2024. Network of thermal cracks in meteorites due to temperature variations: new experimental evidence and implications for asteroid surfaces. MNRAS 500, 1905.
Hamann, C., et al., 2023. Experimental evidence for shear-induced melting and generation of stishovite in granite at low (<18 GPa) shock pressure. JGR: Planets **128** (6), e2023JE007742.
Hamm, M., et al., 2020. Thermophysical modelling and parameter estimation of small solar system bodies via data assimilation. MNRS 496, 2776–2785.
Hamm, M., Grott, M., Senshu, H., et al., 2022. Mid-infrared emissivity of partially dehydrated asteroid (162173) Ryugu shows strong signs of aqueous alteration. Nat. Commun. 13, 364. https://doi.org/10.1038/s41467-022-28051-y.
Hamm, M., Hamilton, V.E., Goodrich, C., 2023. Evidence for the presence of thin and Heterogenous dust deposits on Ryugu's boulders from Hayabusa2 MARA and Sample data. GRL 50, e2023GL10479.
Ho, T.-M., et al., 2021. The MASCOT lander aboard Hayabusa2: the in-situ exploration of NEA (162173) Ryugu. Planet. Space Sci. 200, 105200.
Hörz, Friedrich, 1969. Structural and mineralogical evaluation of an experimentally produced impact crater in granite. Contrib. Mineral. Petrol. 21, 365–377.
Ishizaki, T., et al., 2023. Measurement of microscopic thermal diffusivity distribution for Ryugu sample by infrared lock-in periodic heating method. Int. J. Thermophys. 44 (4), 51.
Jaumann, R., et al., 2019. Images from the surface of asteroid Ryugu show rocks similar to carbonaceous chondrite meteorites. Science 365, 817–820.
Kenkmann, T., et al., 2018. Experimental impact cratering:: a summary of the major results of the MEMIN research unit. Meteorit. Planet. Sci. 53 (8), 1543–1568.
Kitazato, K., et al., 2021. Thermally altered subsurface material of asteroid (162173) Ryugu. Nat. Astron. 5, 246–250.
Kurosawa, K., Ono, H., Niihara, T., 2022. Shock recovery with decaying compressive pulses: shock effects in calcite (CaCO3) around the Hugoniot elastic limit. JGR: Planets 127, e2021JE007133.
Lucchetti, A., et al., 2024. Fast boulder fracturing by thermal fatigue detected on stony asteroids. Nat. Comm. 15, 5206.
Molaro, J.L., Byrne, S., Le, J.L., 2017. Thermally induced stresses in boulders on airless body surfaces, and implications for rock breakdown. Icarus 294, 247–261.
Michel, P., Delbo, M., 2010. Orbital and thermal evolutions of four potential targets for a sample return space mission to a primitive near-Earth asteroid. Icarus 209 (2), 520–534.
Molaro, J.L., et al., 2020. In situ evidence of thermally induced rock breakdown widespread on Bennu's surface. Nat. Commun. 11, 2913.
Müller, T.G., et al., 2017. Hayabusa-2 mission target asteroid 162173 Ryugu (1999 JU3): searching for the object's spin-axis orientation. A&A 599, A103. https://doi.org/10.1051/0004-6361/201629134.
Nakamura, T., et al., 2022. Formation and evolution of carbonaceous asteroid Ryugu: direct evidence from returned samples. Science 379, 6634. https://doi.org/10.1126/science.abn8671.
Okada, T., et al., 2020. Highly porous nature of a primitive asteroid revealed by thermal imaging. Nature 579, 518–522.
Opeil, C.P., et al., 2020. The surprising thermal properties of CM carbonaceous chondrites. Meteorit. Planet. Sci. 55. https://doi.org/10.1111/maps.13556.
Persson, B.N.J., Biele, J., 2022. Heat transfer in granular media with weakly interacting particles. AIP Adv. 12 (10), 105307.
Poelchau, M.H., et al., 2013. The MEMIN research unit: scaling impact cratering experiments in porous sandstones. Meteorit. Planet. Sci. 48, 8–22.
Polanskey, C.A., Ahrens, T.J., 1990. Impact spallation experiments: fracture patterns and spall velocities. Icarus 87, 140–155.
Raith, M., et al., 2018. Nondestructive imaging of hypervelocity impact-induced damage zones beneath laboratory-created craters by means of ultrasound travel-time tomography. Meteorit. Planet. Sci. 53, 1756–1772.
Rozitis, B., et al., 2020. Asteroid (101955) Bennu's weak boulders and thermally anomalous equator. Sci. Adv. 6, 3699.
Ryan, A., et al., 2024. Rocks with extremely low thermal inertia at the OSIRIS-REx sample site on asteroid Bennu. Planet. Sci. J. 5, 92. https://doi.org/10.3847/PSJ/ad2dff.
Sakatani, N., et al., 2021. Anomalously porous boulders on (162173) Ryugu as primordial materials from its parent body. Nat. Astron. 5, 766–774.
Schirner, L., et al., 2024. Aligned fractures on asteroid Ryugu as an indicator of thermal fracturing. A&A 684, A5.
Senshu, H., et al., 2022. Development of numerical model of the thermal state of an asteroid with locally rough surface and its application. Int. J. Thermophys. 43, 102. https://doi.org/10.1007/s10765-022-03030-z.
Shimaki, Y., et al., 2020. Thermophysical properties of the surface of asteroid 162173 Ryugu: infrared observations and thermal inertia mapping. Icarus 348, 113835.
Sugita, S., et al., 2019. The geomorphology, color, and thermal properties of Ryugu: implications for parent-body processes. Science 364, eaaw0422. https://doi.org/10.1126/science.aaw0422.
Watanabe, S., et al., 2019. Hayabusa2 arrives at the carbonaceous asteroid 162173 Ryugu - a spinning top–shaped rubble pile. Science 364, eaav8032. https://doi.org/10.1126/science.aav8032.
Winkler, R., et al., 2018. Subsurface deformation of experimental hypervelocity impacts in quartzite and marble targets. Meteorit. Planet. Sci. 53, 1733–1755.
Yada, T., et al., 2022. Preliminary analysis of the Hayabusa2 samples returned from C-type asteroid Ryugu. Nat. Astron. 6, 214–220. https://doi.org/10.1038/s41550-021-01550-6.
Yokoyama, T., et al., 2023. Samples returned from the asteroid Ryugu are similar to Ivuna-type carbonaceous meteorites. Science 379, eabn7850. https://doi.org/10.1126/science.abn7850.